Biosensors and Bioelectronics 257 (2024) 116334



Contents lists available at ScienceDirect

Biosensors and Bioelectronics

journal homepage: www.elsevier.com/locate/bios



Magnetically modified bacteriophage-triggered ATP release activated EXPAR-CRISPR/Cas14a system for visual detection of *Burkholderia pseudomallei*

Juan Yao [a,b,1], Zhang Zhang [c,1], Hua Pei [d], Ting Zhang [a], Yuping Ruan [a], Chenyuan Liu [c], Yongcan Guo [b,**], Shuo Gu [c,***], Qianfeng Xia [a,*]

[a] NHC Key Laboratory of Tropical Disease Control, School of Tropical Medicine, Hainan Medical University, Haikou, Hainan, 571199, PR China
[b] Nanobiosensing and Microfluidic Point-of-Care Testing, Key Laboratory of Luzhou, Department of Clinical Laboratory, The Affiliated Traditional Chinese Medicine Hospital, Southwest Medical University, Luzhou, Sichuan, 646000, PR China
[c] Department of Neurosurgery, Neurology Center, The First Affiliated Hospital of Hainan Medical University, Haikou, Hainan, 571199, PR China
[d] Department of Clinical Laboratory, The Second Affiliated Hospital, Hainan Medical University, Haikou, Hainan, 571199, PR China

ARTICLE INFO

Keywords:
Melioidosis
Global prevalence
Exponential amplification reaction
Dual amplification
On-site environmental monitoring

ABSTRACT

Burkholderia pseudomallei, widely distributed in tropical and subtropical ecosystems, is capable of causing the fatal zoonotic disease melioidosis and exhibiting a global trend of dissemination. Rapid and sensitive detection of *B. pseudomallei* is essential for environmental monitoring as well as infection control. Here, we developed an innovative biosensor for quantitatively detecting *B. pseudomallei* relies on ATP released triggered by bacteriophage-induced bacteria lysis. The lytic bacteriophage vB_BpP_HN01, with high specificity, is employed alongside magnetic nanoparticles assembly to create a biological receptor, facilitating the capture and enrichment of viable target bacteria. Following a brief extraction and incubation process, the captured target undergoes rapid lysis to release contents including ATP. The EXPAR-CRISPR cascade reaction provides an efficient signal transduction and dual amplification module that allowing the generated ATP to guide the signal output as an activator, ultimately converting the target bacterial amount into a detectable fluorescence signal. The proposed bacteriophage affinity strategy exhibited superior performance for *B. pseudomallei* detection with a dynamic range from 10^2 to 10^7 CFU mL^{-1}, and a LOD of 45 CFU mL^{-1} within 80 min. Moreover, with the output signal compatible across various monitoring methods, this work offers a robust assurance for rapid diagnosis and on-site environmental monitoring of *B. pseudomallei*.

1. Introduction

Burkholderia pseudomallei (*B. pseudomallei*) is a Gram-negative saprophytic bacterium widely distributed in tropical and subtropical environments, gaining significant attention for causing severe zoonotic melioidosis (Gassiep et al., 2020; Wiersinga et al., 2018). The presence of *B. pseudomallei* in the environment poses dual potential threats including the infection risk among populations through various exposures with seasonal variations (Chen et al., 2015), and potential harm to animals and plants, affecting agriculture and ecosystems (Meumann et al., 2024). Model-based estimates suggest approximately 165,000 global melioidosis cases annually, leading to about 89,000 deaths (Limmathurotsakul et al., 2016). Additionally, due to its high pathogenicity and potential for dispersal, *B. pseudomallei* could be misused as a biological weapon in bioterrorist attacks (Brightman and Locum, 2020; Peacock et al., 2008). Accurate detection technology is the primary approach to prevent and control the harm caused by *B. pseudomallei*. Currently, many strategies have been developed to detect *B. pseudomallei* based on bacterial culture (Hoffmaster et al., 2015; Limmathurotsakul et al., 2010), antigen-antibody immune responses (Duval et al., 2014;

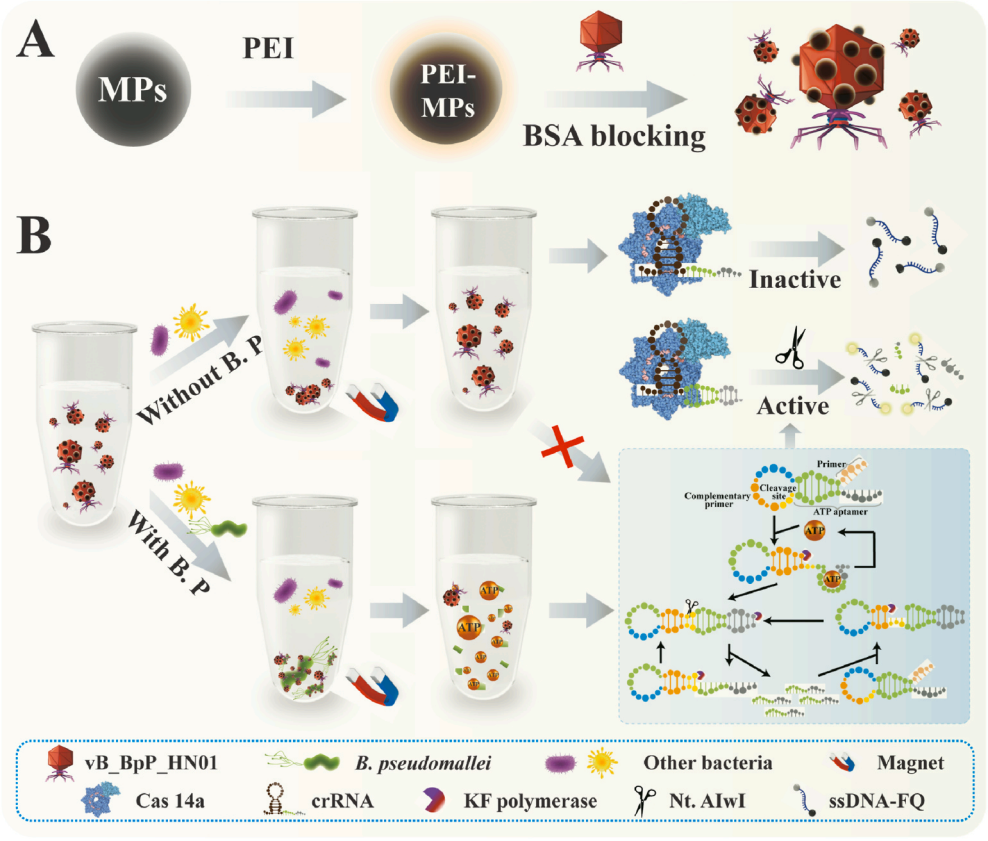
* Corresponding author.
** Corresponding author.
*** Corresponding author.
E-mail addresses: swtcmlab@163.com (Y. Guo), gushuo007@hainmc.edu.cn (S. Gu), xiaqianfeng@hainmc.edu.cn (Q. Xia).
[1] Juan Yao and Zhang Zhang contributed equally to this work.

https://doi.org/10.1016/j.bios.2024.116334
Received 13 January 2024; Received in revised form 19 April 2024; Accepted 24 April 2024
Available online 25 April 2024
0956-5663/© 2024 Elsevier B.V. All rights reserved.

Muangsombut et al., 2021), mass spectrometry analysis (Watthanaworawit et al., 2021), serological tests including indirect hemagglutination assay (IHA), enzyme-linked immunosorbent assay (ELISA), and immunofluorescence assay (IFA) (Chaichana et al., 2018; Hodgson et al., 2009; Suttisunhakul et al., 2016; Torres et al., 2020), and molecular biology techniques (Chantratita et al., 2007; Meumann et al., 2006). Recently, new rapid diagnostic technologies for *B. pseudomallei* nucleic acids have been gradually developed (Li et al., 2023; Yao et al., 2023). Unfortunately, these technologies are time-consuming or depend on specialized laboratory equipment and skilled operation, making them difficult to meet the needs of rapid field detection. Meanwhile, the global prevalence of *B. pseudomallei* is severely underestimated due to limited diagnostic approaches in laboratories and insufficient expertise (Savelkoel et al., 2022). Therefore, developing a simple, sensitive, and specific novel diagnostic technology for *B. pseudomallei* is crucial for melioidosis infection control and environmental monitoring.

Bacteriophages are viruses capable of infecting a range of microorganisms, and exhibiting high specificity and selectivity to infect and lyse target bacteria while sparing other microorganisms from harm (Secor and Dandekar, 2020; Sharma et al., 2017). Compared to the high production costs and strict storage conditions required for antibodies, bacteriophages can overcome these limitations, which renders them potential tools for biological detection (Nobrega et al., 2018; Paul, 2023). Researchers have utilized the bio-recognition properties of bacteriophages to develop diverse methods for bacterial detection, achieving highly sensitive bacterial detection (Arnaud et al., 2017). Furthermore, analyzing specific substances released during the process of bacteriophage-induced lysis such as adenosine triphosphate (ATP) and β-galactosidase, whether qualitatively or quantitatively, can aid in identifying bacterial species (Corbitt et al., 2000; Neufeld et al., 2003). In our previous research, a bacteriophage named vB_BpP_HN01 of *B. pseudomallei* was isolated from Hainan Province for the first time in China (Wang et al., 2022). Research indicates that the bacteriophage exhibit excellent stability and a broad-spectrum lytic ability, showcasing significant potential in the diagnosis of *B. pseudomallei* infections on Hainan Island.

ATP is a universally present biomolecule in living organisms. Active bacteria continuously generate ATP to sustain their metabolic activities. As a widely employed method in the fields of water quality testing and food hygiene detection (Esimbekova et al., 2022), ATP bioluminescence assay indirectly evaluates the presence and activity of bacteria by measuring ATP catalytic bioluminescence intensity, but it also has defects such as poor specificity and susceptibility to sample handling and environmental factors (Zhang et al., 2017). Unlike bioluminescence analysis, the aptamer-based analysis determines the actual number of biomolecules. Aptamers are nucleic acid or peptide molecules obtained through in vitro screening that specifically bind to a target molecule, their editable and flexible transforming capabilities give them potential applications in therapeutics and diagnostics (Liu et al., 2009). In 1993, a RNA aptamer for ATP was initially screened out by Szostak (Sassanfar and Szostak, 1993), laying the foundation for the study of ATP biosensors. However, the sensitivity of ATP aptamer-based biosensors are limited to micromolar levels, falling short of meeting the requirements for monitoring extremely low bacterial counts (Li et al., 2022; Xiong et al., 2019). In the design of biosensors, the nucleic acid properties of the aptamers can be exploited to improve the sensitivity by increasing the number of targets. Exponential amplification reaction (EXPAR) is an isothermal nucleic acid amplification technique that utilizes the chain displacement activity of polymerase to replace one strand in dsDNA (Reid et al., 2018). It could rapidly amplify short oligonucleotides, called triggers, in less than 10 min and has been utilized for the detection of various targets, including nucleic acids, proteins, and enzymes, due to



Scheme 1. Schematic illustrating of vB-MPs mediated *B. pseudomallei* detection. (A) Fabrication process of vB-MPs. (B) Schematic illustration of the dual-amplification strategy for *B. pseudomallei* detection with EXPAR-CRISPR/Cas system.

its simplicity, sensitivity, and speed. Additionally, EXPAR has been applied for ultrarapid detection of pathogens and demonstrated enormous potential in point-of-care testing and on-site analysis. The limitation of non-specific amplification can also be addressed through clever template chain structure design (Chen et al., 2021). Another way to increase the sensor sensitivity is to amplify the output signal. Clustered regularly interspaced short palindromic repeats (CRISPR)/Cas system is a revolutionary gene-editing technology derived from bacterial immune systems. In addition to allowing the precise editing of DNA sequences, the recognition and binding of the guide RNA to the target sequence is also able to further activate both cis- and trans-cleavage activities of Cas protein, which holding immense potential in various fields like medicine and biotechnology (Gootenberg et al., 2018; Ma et al., 2023a). Importantly, most cas proteins exhibit optimal recognition and cleavage activities at 37 °C, enabling their combined application with low-temperature nucleic acid amplification techniques for sensitive target detection (Ma et al., 2023b).

In this study, an innovative biosensor for quantitative detection of *B. pseudomallei* based on the ATP release induced by magnetically modified vB_BpP_HN01 was proposed, and the feasibility and performance parameters of this method are also demonstrated. Leveraging the high specificity of bacteriophages and the dual amplification strategy involving EXPAR-CRISPR/Cas system, it enables rapid and sensitive detection of *B. pseudomallei* in patient and environmental samples.

2. Experimental section

Limited to the word count requirements, the experimental sections have been put in the supplementary material.

3. Results and discussion

3.1. Working principle of the detection scheme

The schematic illustrates an innovative biosensor designed for sensitive, specific, and rapid detection of *B. pseudomallei* (Scheme 1). Initially, MPs were modified with PEI to acquire a dense positive charge, which facilitated electrostatic adsorption and immobilization on the head of vB_BpP_HN01, resulting in the formation of vB-MPs (Wang et al., 2022). After incubating functionalized vB-MPs with samples under optimal conditions for target binding, a magnetic separation device is applied to separate bound particles. Subsequent washing steps enable vB-MPs to selectively capture and enrich *B. pseudomallei* targets, enhancing detection sensitivity. Upon injection of bacteriophage DNA and progeny replication and assembly, the host bacteria underwent eventual lysis, resulting in the release of progeny bacteriophages and abundant bacterial contents, including ATP. The interaction between ATP and aptamer-template induces a conformational change, exposing binding sites for KF polymerase and endonuclease. It leads to a significant amplification of activator DNA, transitioning from ATP detection to the detection of nucleic acids. The activator DNA was served as a recognition target for crRNA to induce the cleavage activity of the Cas14a protein, ultimately producing a detectable fluorescence signal. The fluorescence signal intensity showed a positive correlation with the initial content of host bacteria in the sample. Conversely, in the absence of *B. pseudomallei*, the capture and enrichment processes of vB-MPs did not take place. As a result, subsequent signal output were hindered. This approach capitalizes on the high specificity of vB_BpP_HN01 and a dual signal amplification strategy guided by ATP, enabling accurate and sensitive detection of target bacteria at trace levels.

3.2. Preparation, characterization, and biological property analysis of vB-MPs

The bacterial detection scheme, built upon lytic bacteriophages, depends on their precise recognition and swift lysis of the host bacteria. vB_BpP_HN01 was the first bacteriophage of *B. pseudomallei* in China and isolated from Dongfang City, Hainan Province, and its genomic information and biological characteristics have been reported in detail (Wang et al., 2022). A typical phage plaque assay was conducted by combining various proportions of vB_BpP_HN01 with *B. pseudomallei* to create double-layer agar plates (Fig. 1A). The results indicate that vB_BpP_HN01 is capable of lysing the host bacteria and generates progeny under suitable bacterial growth conditions. Structural images obtained through TEM revealed that vB_BpP_HN01 consists of an icosahedral symmetric head ($\Phi = 62.0 \pm 1.3$ nm) and a typical short tail (20.4 ± 0.7 nm), classifying it under the *Podoviridae* family (Fig. 1BCE). To achieve effective bacteria enrichment, the MPs with unique magnetic properties were utilized to prepare vB-MPs. As shown in Fig. 1Ba and 1Bb, MPs, initially 20 nm in diameter with a smooth surface, show increased diameter to 22 nm with a hydration membrane after PEI modification. FTIR spectra (Fig. S1) displays characteristic N–H stretching vibration absorption peaks at 3422 cm^{-1} for both PEI and PEI@MPs compared to original MPs (Gao et al., 2022). Zeta potential results show that the surface charge of modified MPs increased from 20.3 ± 0.89 mV to 46.3 ± 1.71 mV (Fig. 1C). Owing to the negative charge on the head of vB_BpP_HN01 ± 0.4 mV), MPs can be immobilized onto vB_BpP_HN01's surface through electrostatic adsorption (Fig. 1Bd). The satisfactory binding efficiency of PEI@MPs to vB_BpP_HN01 was verified by fluorescence quantitative PCR, and the experimental details has been put in the supplementary material (Fig. S2). The lytic ability of vB-MPs on *B. pseudomallei* were assessed by standard plaque assay. Fig. 1D displays plaque images under different treatment conditions, where MPs alone failed to generate plaques either before or after ultrasonic treatment. Binding of vB_BpP_HN01 to MPs without PEI modification results in dark plaques, which decreased after ultrasonic treatment, suggesting an unstable association between bacteriophages and unmodified MPs. vB-MPs generates distinguishable plaques, and the plaques persist unaffected following ultrasonic treatment. The specificity and lysis spectrum of vB-MPs was also be verified through plaque assay, which demonstrating an extensive lytic effect on *B. pseudomallei* (Figs. S3 and S4). The aforementioned lysis process underlies the release of cellular contents, including ATP, which facilitates the establishment of a detection system for *B. pseudomallei*.

3.3. Construction and feasibility of the EXPAR-CRISPR/Cas system for detecting ATP

The ATP recognition and signal conversion system comprise two main parts. Firstly, an amplification system is triggered by the ATP aptamer, inducing a conformational change in the nucleic acid chain that activates EXPAR (Fig. 2A). This system includes a self-priming template with the aptamer region recognizing ATP, followed by the Nt.AIwI recognition site, self-primer sequences, and aptamer's antisense sequence. Initially, the template forms a stable, inactive stem-loop structure. In the presence of ATP, the template undergoes a conformational change, activating EXPAR and initiating dsDNA cleavage by Nt.AIwI. The generated ssDNA, along with released ATP, initiates a new round of amplification, transforming ATP into detectable nucleic acids. Fluorescence quantitative PCR was used to validate the feasibility of this system (Fig. 2B). A rapid increase in fluorescence intensity was observed within the range of 13–40 min only in the presence of aptamer-template, ATP, and KF polymerase, which was significantly distinguishable from the non-specific amplification observed in the target-free state. PAGE analysis (Fig. 2C) further confirms ATP-triggered EXPAR. The other part involves the establishment of activator DNA-guided CRISPR/Cas14a signal output system. Cas14a′s cleavage capability is confirmed through fluorescence monitoring (Fig. 2D and E), where high fluorescence and ssDNA-FQ cleavage occurred only in the coexistence of Cas14a, crRNA, activator DNA, and ssDNA-FQ. The fluorescence intensity correlates linearly with activator DNA concentration (2.5–80 nM).

The capability of the EXPAR-CRISPR/Cas14a system for ATP

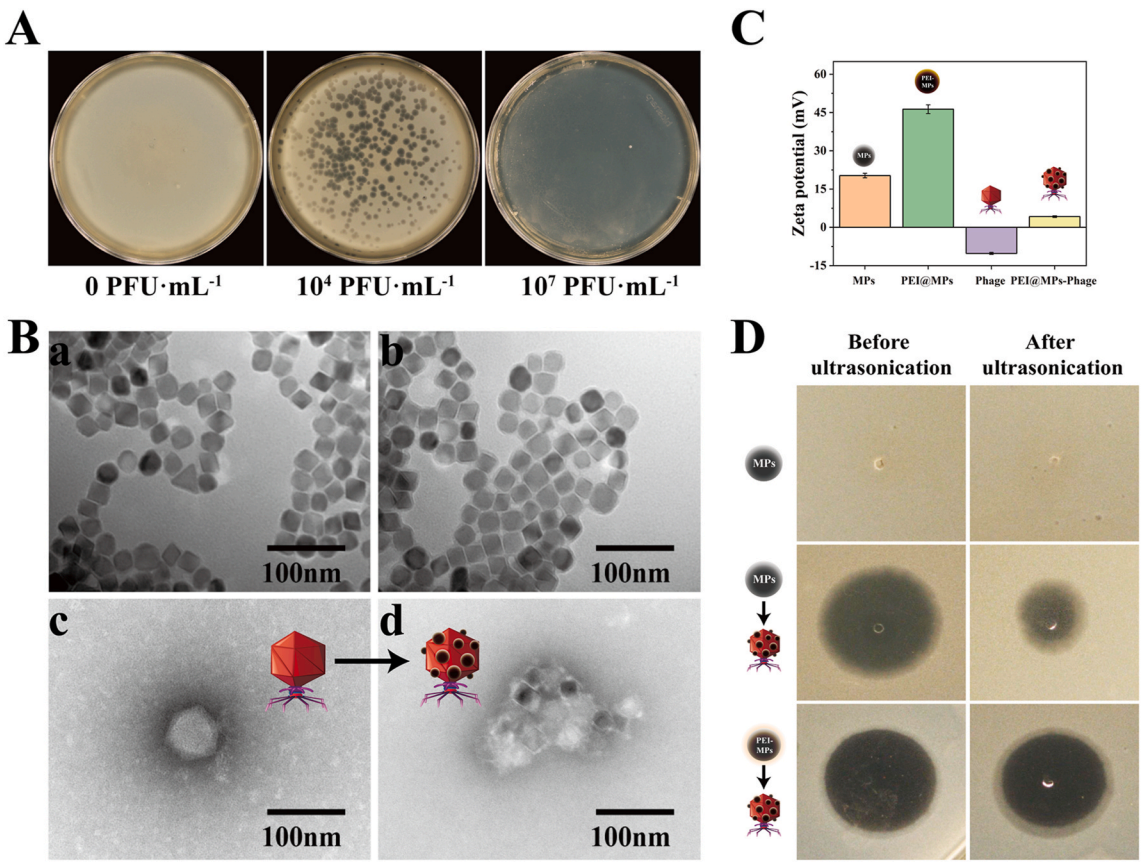


Fig. 1. Characterization and biological property analysis of vB_BpP_HN01 and vB-MPs. (A) Plaques produced by different concentrations of vB_BpP_HN01 and *B. pseudomallei* (10ˆ8 CFU mL^{-1}) mixture. (B) TEM images of MPs (a), PEI@MPs (b), vB_BpP_HN01 (c) and vB-MPs (d). (C) Zeta potential of MPs, PEI@MPs, vB_BpP_HN01 and vB-MPs (n = 3). (D) Plaques produced under different treatment towards *B. pseudomallei* before and after ultrasonication.

detection is confirmed through PAGE analysis and fluorescence spectrum data. In Fig. 2F, ssDNA-FQ was digested when co-incubated with Cas14a-crRNA and activator DNA (lane 4), resulting in reduced brightness. Co-incubation of the aptamer-template in stem-loop structure with Cas14a-crRNA did not lead to the cleavage of ssDNA-FQ (lane 5). In the presence of ATP, similar cleavage result to those in lane 4 was observed (lane 6), indicating that Cas14a was activated by activator DNA generated from ATP-triggered EXPAR. Similar conclusions can also be observed in fluorescence spectrum data (Fig. 2G). Optimization of reaction conditions reveals the best performance with specific concentrations of KF polymerase (0.1 U·mL^{-1}), Nt. AIwI (0.2 U·mL^{-1}), Cas14a (40 nM), crRNA (40 nM), and ssDNA-FQ (100 nM) (Figs. S5 and S6). To quantitatively detect ATP with EXPAR-CRISPR/Cas14a system, we measured fluorescence spectra with the addition of various concentrations of ATP. Fig. 2H demonstrates a linear fluorescence signal within the range of 10ˆ2 aM to 10ˆ7 aM, with a LOD of 39 aM. The system also exhibits excellent specificity for ATP, AMP, and ADP, ensuring accurate detection results (Fig. 2I) and avoiding signal loss due to by-products generated during ATP metabolism (Lomakina et al., 2015).

3.4. Feasibility and optimization of vB-MPs mediated B. pseudomallei detection

As a crucial intracellular component, the quantity of ATP released during bacterial lysis directly reflects the original bacterial quantity (Selan et al., 1992). Fig. 3A illustrates the workflow of this strategy briefly. The mixture containing target bacteria was co-incubated with vB-MPs. After magnetic separation to isolate and enrich targets, the supernatant obtained after a brief lysis process can be used for subsequent detection in EXPAR-CRISPR/Cas14a system. Fig. 3B depicts the fluorescence signal changes in the supernatant of standard solutions containing different concentrations of *B. pseudomallei* and PBS (used as a blank control) after capture and lysis treatment in EXPAR-CRISPR/Cas14a system. It exhibits a significant difference from the negative control and the fluorescence intensity is closely correlated with the bacterial concentration. As the incubation time of vB-MPs with *B. pseudomallei* significantly affects the quantity of trapped host bacteria, and the combined influence of lysis time on ATP release, these two parameters were optimized using *B. pseudomallei* standard solution with a concentration of 10ˆ7 CFU mL^{-1}. As shown in Fig. 3C and D, the optimal signal-to-noise ratio was achieved with an incubation time of 10 min for vB-MPs with *B. pseudomallei* and a lysis time of 30 min. Excessively short times may result in insufficient capture of bacteria or incomplete lysis, while long times can lead to ATP leakage and metabolic losses. To facilitate the application of this strategy in portable detection devices, we determined a reaction time of 30 min which maximizes the signal-to-noise ratio, to obtain the optimal ATP output signal (Fig. 3E). Furthermore, the reaction temperature of the entire system was optimized, and the results indicated that the optimal detection performance was achieved under the conditions of 37 °C (Fig. S7). This was attributed to the fact that several enzymes involved in the reaction system can maintain their optimal activity at 37 °C.

3.5. Performance of vB-MPs mediated B. pseudomallei detection

We conducted a detailed analysis of the analytical performance of the established platform for detecting *B. pseudomallei*. *B. pseudomallei* standard solutions of various concentrations were prepared and tested with the platform following the previously described procedure under optimized conditions. Fig. 4A illustrates a significant change in

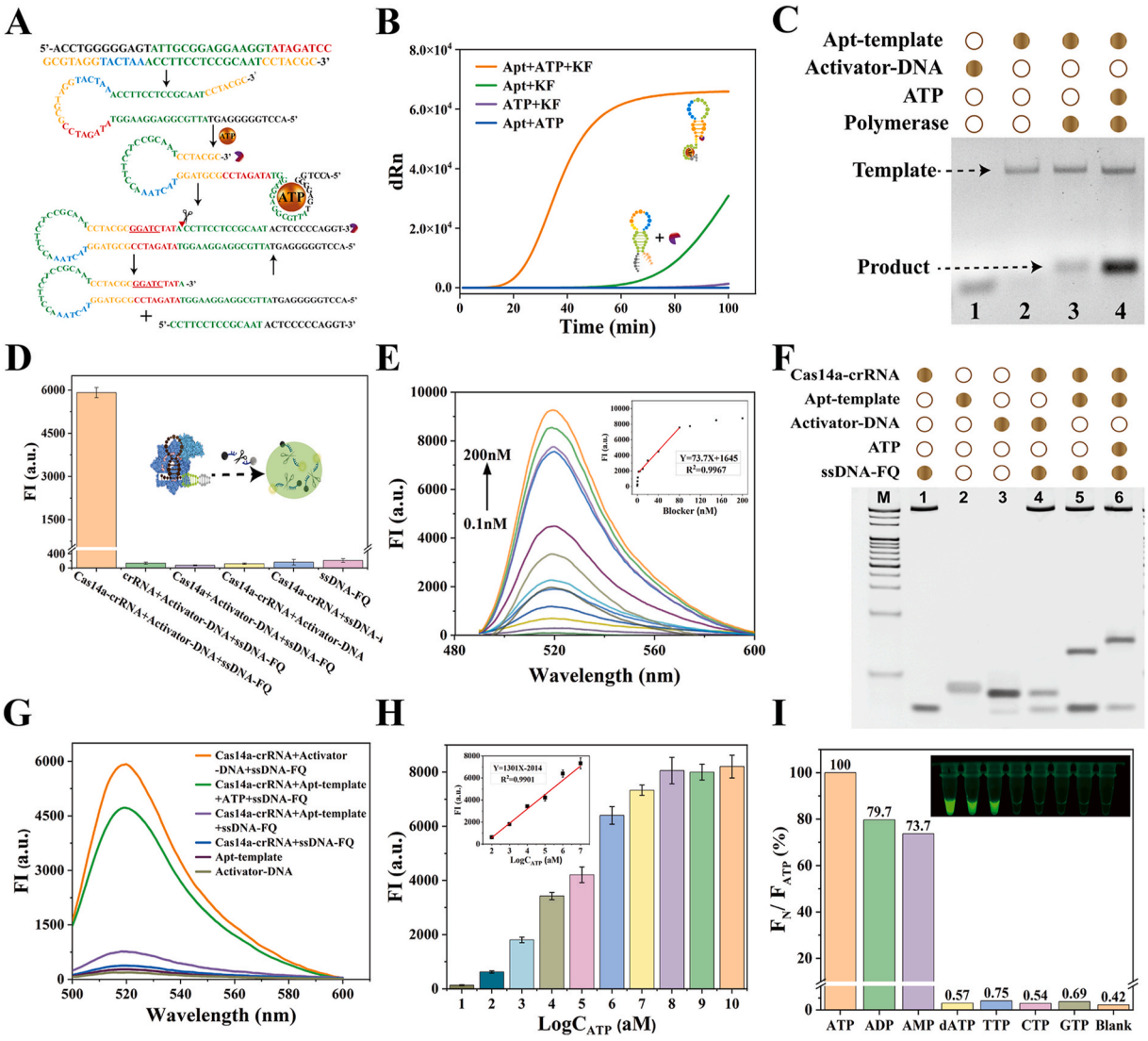


Fig. 2. Construction and feasibility of the EXPAR-CRISPR/Cas14a system for detecting ATP. (A) Design and DNA sequence of aptamer-template used in EXPAR for ATP detection. (B) Real-time fluorescence monitoring of EXPAR in different groups of Apt (aptamer template DNA, 1 μM), ATP and KF (KF polymerase, 5 U·μL^{-1}). (C) PAGE analysis of EXPAR. (D) Feasibility validation of CRISPR/Cas14a-guided fluorescence signal output (Cas14a 40 nM, crRNA 40 nM, activator DNA 40 nM, and ssDNA-FQ 100 nM) (n = 3). (E) Effects of different activator DNA concentrations (0.1–200 nM) on CRISPR/Cas14a-guided signal output. (F) PAGE analysis and (G) fluorescence spectra of the feasibility of ATP-induced EXPAR-CRISPR/Cas14a activation. (H) Fluorescence signal increase in buffer over different concentration of ATP, ranging from 10^1–10^10 aM. Inset: standard curve for ATP detection in EXPAR-CRISPR/Cas14a system. (n = 3) (I) Specificity of ATP detection. All components concentrations were indicated as 10^6 aM. Inset: the fluorescent images of different component in EXPAR-CRISPR/Cas14a system.

fluorescence intensity with the increase of *B. pseudomallei* concentration, indicating the platform's satisfactory responsiveness to the target bacteria. The linear detection range of this method for *B. pseudomallei* is 1.8 × 10^2 to 1.8 × 10^7 CFU mL^{-1}, expressed by the linear regression equation FI (a.u.) = 1377LogC-1565 (where FI is the detected fluorescence intensity, and C is the concentration of *B. pseudomallei*). The relative standard deviation (RSD) values for *B. pseudomallei* standard samples at low (1.8 × 10^2 CFU mL^{-1}), medium (1.8 × 10^5 CFU mL^{-1}), and high (1.8 × 10^7 CFU mL^{-1}) concentrations were measured to be 5.7%, 3.5%, 2.1%, respectively. The correlation coefficient (R^2) is 0.9926, and LOD for *B. pseudomallei* is 45 CFU mL^{-1} (Fig. 4B). To assess the specificity of this method, several other interfering strains (*E. faecalis, S. aureus, P. aeruginosa, E. coli, S. maltophilia, K. pneumoniae, and B. cepacia*) alongside *B. pseudomallei* were simultaneously tested at the concentration of 10^7 CFU mL^{-1}. In comparison to the host strain, there was little increase in fluorescence signal observed in these interfering and blank samples. It provides additional evidence for the satisfactory specificity of the proposed method, mainly owing to the high selectivity of vB_BpP_HN01 for *B. pseudomallei* (Fig. 4C). We applied both PCR and our proposed method to 40 randomly selected samples, including 16 negatives and 24 positives, to assess the practical applicability. Fig. 4D illustrates that our constructed strategy detected 23 positive samples with a sensitivity of 95.8% (23/24) and specificity of 100% (16/16). The performance surpassed that of the PCR targeting the Type III secretion system gene (T3SS) fragment, which achieved a sensitivity of 91.6% (22/24) and specificity of 81.3% (13/16). All positive samples demonstrated higher fluorescence intensity than the remaining negative samples. The receiver operating characteristic curve (ROC) indicated that the area under the curve (AUC) of our strategy was superior to that of PCR, providing further evidence of the proposed method's superior performance (Fig. 4E).

3.6. Application of vB-MPs mediated B. pseudomallei detection in environmental samples

As an environmental saprophyte, *B. pseudomallei* causes the severe

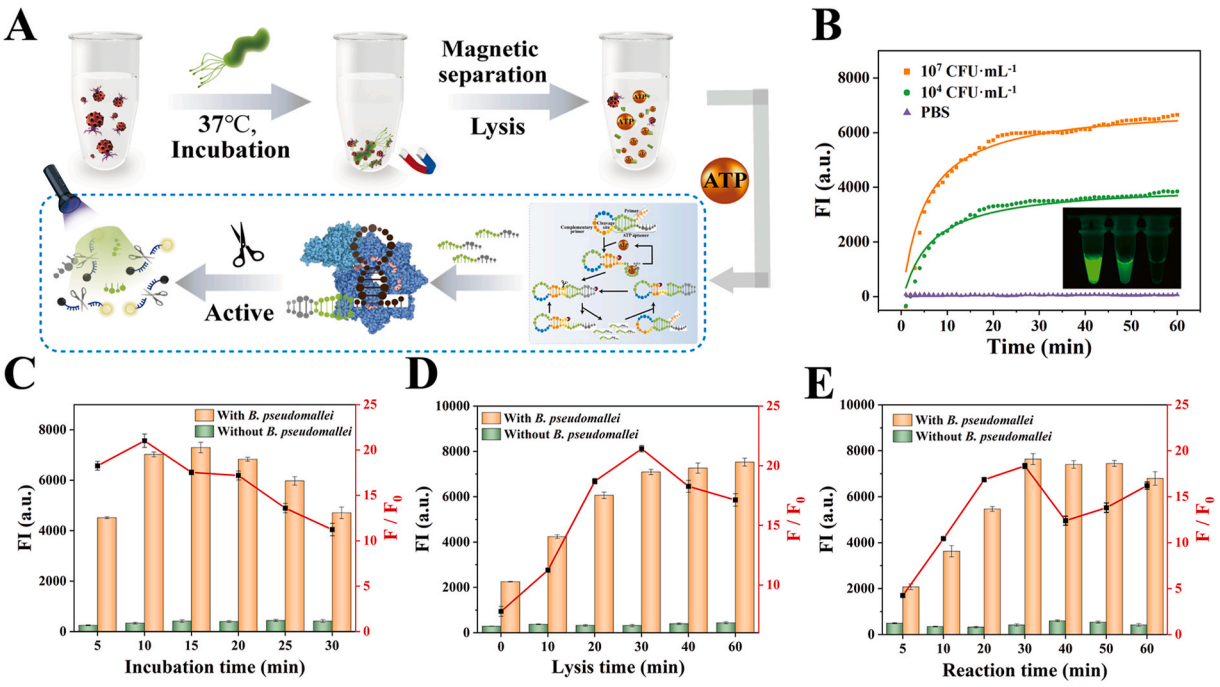


Fig. 3. Feasibility and optimization of vB-MPs mediated *B. pseudomallei* detection. (A) Workflow of vB-MPs mediated *B. pseudomallei* detection. (B) Fluorescence signal changes in EXPAR-CRISPR/Cas14a system mixing with the supernatant of different concentrations of *B. pseudomallei* and PBS (used as a blank control). Inset: the fluorescent images of different concentrations of *B. pseudomallei* and PBS. Optimization of incubation time (C), lysis time (D) and reaction time (E) in vB-MPs mediated *B. pseudomallei* detection. The concentration of the *B. pseudomallei* standard solution used in optimization experiment was 10^7 CFU mL^{-1} (F represented the fluorescence intensity measured after reaction, F_0 represented the fluorescence intensity of blank control). All other conditions were the chosen optimal conditions (n = 3).

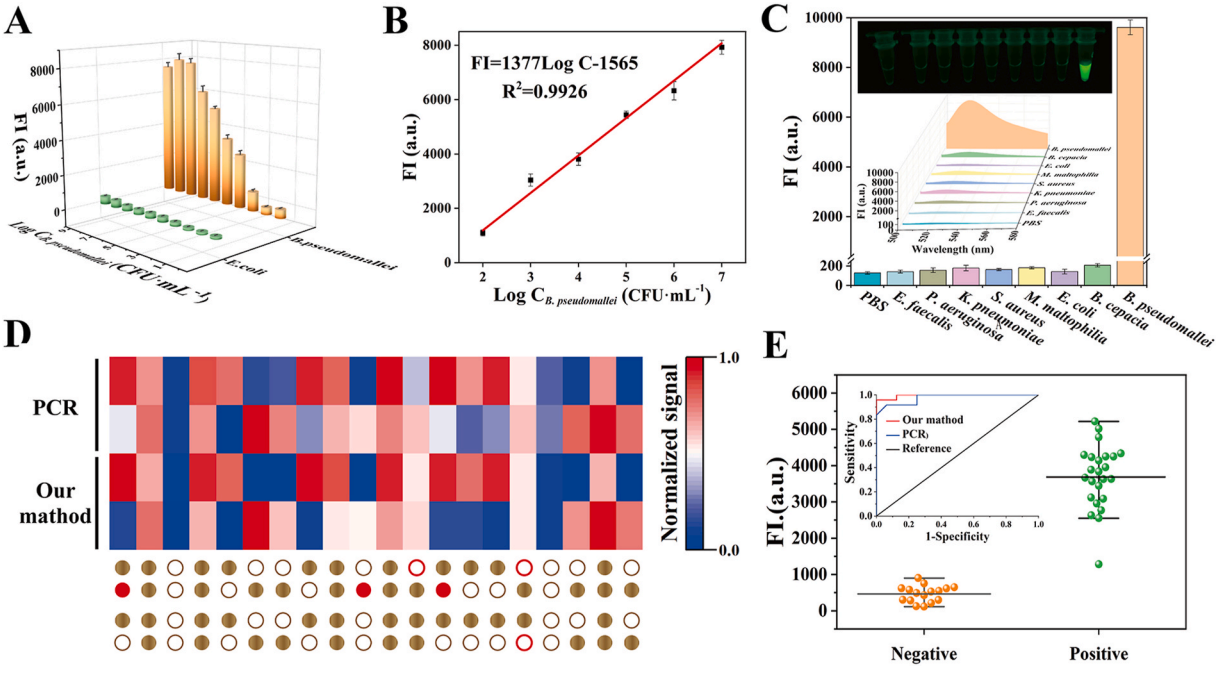


Fig. 4. Performance of vB-MPs mediated *B. pseudomallei* detection. (A) Fluorescent readouts with excitation at 490 nm and emission at 520 nm of *B. pseudomallei* and *E. coli* samples with different concentrations, respectively. (n = 3).(B) Calibration curves of the proposed strategy in detecting different concentrations of *B. pseudomallei* in PBS buffer. (C) The selectivity of the proposed strategy for detecting *B. pseudomallei* and other common reference strains. Inset: fluorescent spectra and fluorescent images of *B. pseudomallei* and other common reference strains. (n = 3) (D) Thermal analysis chart of *B. pseudomallei* detected by the proposed strategy and PCR. Brown solid dots: true positive samples; brown hollow circles: true negative samples; red solid dots: false positive samples; red hollow circles: false negative samples. (E) Fluorescence intensity of all positive samples and negative samples. Inset: comparison of the ROC analysis between the proposed strategy and PCR.(For interpretation of the references to colour in this figure legend, the reader is referred to the web version of this article.)

infectious disease melioidosis, which is closely linked to exposure to contaminated water sources, products, and the environment (Meumann et al., 2024). It poses a significant threat, especially to immunocompromised individuals. We evaluated the potential application of the developed platform for detecting *B. pseudomallei* in environmental samples. Various environmental samples with known concentrations were created by adding different amounts of *B. pseudomallei* standard solution to pure water and sewage, serving as the environmental matrix. The concentration of *B. pseudomallei* in these samples was then determined using the developed platform to evaluate their recovery rate. The results listed in Table S2 show that the recovery of samples with added *B. pseudomallei* was in the range of 75.7%–97.3% with RSD values in the range of 3.2%–9.7%. Fig. 5A shows an increase in fluorescence signals with rising concentrations of *B. pseudomallei* in both pure water and sewage. In order to make the method realize on-site environmental monitoring, portable fluorescence monitoring device was used to visually observe the fluorescence, with images captured by smartphone. (Fig. 4B). In pure water samples, the linear regression equation is FI (a.u.) = 1962LogC-2956 with a linear range of 3.0 × 10^2–3.0 × 10^7 CFU mL^{-1} ($R^2 = 0.99$), and the LOD was 98 CFU mL^{-1} (Fig. 5C), with all RSD values below 6.8 %. In sewage, the linear regression equation is FI (a.u.) = 1783LogC-2664 with a linear range of 3.0 × 10^2–3.0 × 10^7 CFU mL^{-1} ($R^2 = 0.98$), and the LOD was 1.1 × 10^2 CFU mL^{-1} (Fig. 5D), with all RSD values below 8.3 % (where FI is the detected fluorescence intensity, C represents the concentration of *B. pseudomallei* added in the matrix). Furthermore, the constructed system was able to accurately identify *B. pseudomallei* in complex simulated environmental samples (Fig. S8). All these results could indicate the reliability of the proposed strategy for detecting *B. pseudomallei* in environmental samples.

4. Conclusion

In this study, we have devised a rapid, specific, and sensitive method for the detection of *B. pseudomallei*. Leveraging vB_BpP_HN01, we synergistically combine organic biomaterial bacteriophages with inorganic magnetic nanoparticles to enable swift target identification and extraction from clinical and environmental samples. Additionally, the EXPAR-CRISPR/Cas14a system, utilizing aptamer-induced conformational changes, achieves dual amplification from bacterial quantity to detectable signal intensity, thereby enhancing strategy sensitivity. The newly developed method is compatible with various detection platforms including mainstream fluorescence analyzers and other visual technologies, and the entire test process can be completed within 80 min, with a performance range from 1.8 × 10^2 to 1.8 × 10^7 CFU mL^{-1} and a LOD of 45 CFU mL^{-1}. However, it is worth noting that the method's performance may be influenced by the diversity of *B. pseudomallei* strains, warranting further exploration into different lineages. Furthermore, a comprehensive specificity evaluation against broader *B. pseudomallei* complex species and non-target bacteria in environmental samples is crucial for thorough assessment. In summary, our study lays a solid foundation for the rapid identification of *B. pseudomallei,* and continued efforts are essential to address the identified limitations and propel this method towards real-world applications. We envision this research opening doors to advancements in melioidosis diagnosis and environmental monitoring, fostering a deeper understanding of the pathogen's prevalence and facilitating timely interventions.

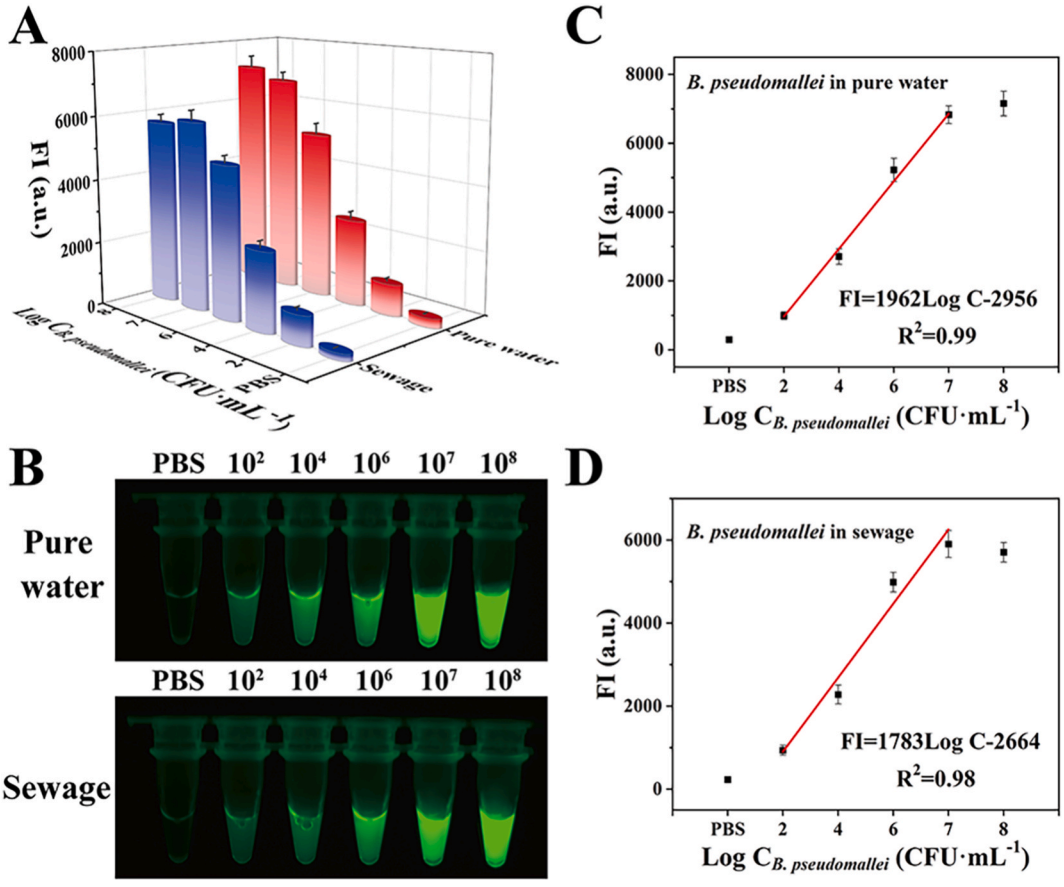


Fig. 5. Application of vB-MPs mediated *B. pseudomallei* detection in environmental samples. (A) Fluorescent readouts with excitation at 490 nm and emission at 520 nm of pure water and sewage samples with different concentrations of *B. pseudomallei*, respectively. (n = 3) (B) The fluorescent images of *B. pseudomallei* in pure water and sewage taken by smartphone. (C) Calibration curves of the proposed strategy in detecting different concentrations of *B. pseudomallei* in pure water. (D) Calibration curves of the proposed strategy in detecting different concentrations of *B. pseudomallei* in sewage.

CRediT authorship contribution statement

Juan Yao: Writing – original draft, Visualization, Methodology, Investigation, Formal analysis, Data curation. **Zhang Zhang:** Validation, Data curation, Conceptualization. **Hua Pei:** Resources, Methodology, Investigation. **Ting Zhang:** Writing – review & editing, Validation. **Yuping Ruan:** Investigation, Data curation. **Chenyuan Liu:** Validation, Formal analysis. **Yongcan Guo:** Writing – review & editing, Resources, Funding acquisition, Conceptualization. **Shuo Gu:** Writing – review & editing, Supervision, Project administration, Funding acquisition. **Qianfeng Xia:** Writing – review & editing, Supervision, Resources, Methodology, Funding acquisition, Conceptualization.

Declaration of competing interest

The authors declare that they have no known competing financial interests or personal relationships that could have appeared to influence the work reported in this paper.

Data availability

Data will be made available on request.

Acknowledgments

We would like to express our gratitude to the staff of the Second Affiliated Hospital of Hainan Medical University and the Affiliated Traditional Chinese Medicine Hospital of Southwest Medical University for their support throughout this research. This work was supported by the Major Science and Technology Program of Hainan Province (ZDKJ202003, ZDKJ2021036), the National Natural Science Foundation of China (Grant No. 82370018, 82272431), Sichuan Science and Technology Program (2023NSFSC1478, 2022YFS0623, 2023ZYD0287), and State Key Research Development Program of China (2022YFC2305000, 2022YFC2305003).

Appendix A. Supplementary data

Supplementary data to this article can be found online at https://doi.org/10.1016/j.bios.2024.116334.

References

Arnaud, C.-A., Effantin, G., Vivès, C., Engilberge, S., Bacia, M., et al., 2017. Nat. Commun. 8 (1), 1953.
Chaichana, P., Jenjaroen, K., Amornchai, P., Chumseng, S., Langla, S., et al., 2018. Am. J. Trop. Med. Hyg. 99 (6), 1378–1385.
Chantratita, N., Wuthiekanun, V., Limmathurotsakul, D., Thanwisai, A., Chantratita, W., et al., 2007. Am. J. Trop. Med. Hyg. 77 (5), 814–817.
Chen, J., Zhu, D., Huang, T., Yang, Z., Liu, B., et al., 2021. Anal. Chem. 93 (37), 12707–12713.
Chen, P.S., Chen, Y.S., Lin, H.H., Liu, P.J., Ni, W.F., et al., 2015. PLoS Neglected Trop. Dis. 9 (6), e0003834.
Corbitt, A., Bennion, N., Forsythe, S., 2000. Lett. Appl. Microbiol. 30 (6), 443–447.
Duval, B.D., Elrod, M.G., Gee, J.E., Chantratita, N., Tandhavanant, S., 2014. Am. J. Trop. Med. Hyg. 90 (6), 1043.
Esimbekova, E.N., Kirillova, M.A., Kratasyuk, V.A., 2022. Biosensors 13 (1), 47.
Gao, M., Zhu, Y., Yan, J., Wu, W., Wang, B., 2022. Membranes 12 (8), 809.
Gassiep, I., Armstrong, M., Norton, R., 2020. Clin. Microbiol. Rev. 33 (2).
Gootenberg, J.S., Abudayyeh, O.O., Kellner, M.J., Joung, J., Collins, J.J., et al., 2018. Science 360 (6387), 439–444.
Hodgson, K., Engler, C., Govan, B., Ketheesan, N., Norton, R., 2009. J. Clin. Microbiol. 47 (5), 1578–1580.
Hoffmaster, A.R., AuCoin, D., Baccam, P., Baggett, H.C., Baird, R., et al., 2015. Emerg. Infect. Dis. 21 (2).
Li, C., Liu, C., Liu, R., Wang, Y., Li, A., et al., 2023. Biosens. Bioelectron. 225, 115098.
Li, X., Chen, X., Mao, M., Peng, C., Wang, Z., 2022. Biosens. Bioelectron. 217.
Limmathurotsakul, D., Golding, N., Dance, Det. al.A., Messina, J.P., Pigott, D.M., et al., 2016. Nat Microbiol 1, 15008.
Limmathurotsakul, D., Jamsen, K., Arayawichanont, A., Simpson, J.A., White, L.J., et al., 2010. PLoS One 5 (8), e12485.
Liu, J., Cao, Z., Lu, Y., 2009. Chem. Rev. 109 (5), 1948–1998.
Lomakina, G.Y., Modestova, Y.A., Ugarova, N., 2015. Biochemistry (Moscow) 80, 701–713.
Ma, L., Wang, J., Li, Y., Liao, D., Zhang, W., et al., 2023a. J. Hazard Mater. 443, 130234.
Ma, L., Zhang, W., Yin, L., Li, Y., Zhuang, J., et al., 2023b. J. Hazard Mater. 452, 131195.
Meumann, E.M., Limmathurotsakul, D., Dunachie, S.J., Wiersinga, W.J., Currie, B.J., 2024. Nat. Rev. Microbiol. 22, 155–169.
Meumann, E.M., Novak, R.T., Gal, D., Kaestli, M.E., Mayo, M., et al., 2006. J. Clin. Microbiol. 44 (8), 3028–3030.
Muangsombut, V., Withatanung, P., Chantratita, N., Chareonsudjai, S., Lim, J., et al., 2021. Appl. Environ. Microbiol. 87 (12).
Neufeld, T., Schwartz-Mittelmann, A., Biran, D., Ron, E., Rishpon, J., 2003. Anal. Chem. 75 (3), 580–585.
Nobrega, F.L., Vlot, M., de Jonge, P.A., Dreesens, L.L., Beaumont, H.J., et al., 2018. Nat. Rev. Microbiol. 16 (12), 760–773.
Paul, S.S., 2023. Prog Mol Biol Transl Sci 200, 91–101.
Peacock, S.J., Schweizer, H.P., Dance, D.A., Smith, T.L., Gee, J.E., et al., 2008. Emerg. Infect. Dis. 14 (7), e2.
Reid, M.S., Le, X.C., Zhang, H., 2018. Angew. Chem. Int. Ed. 57 (37), 11856–11866.
Sassanfar, M., Szostak, J.W., 1993. Nature 364 (6437), 550–553.
Savelkoel, J., Dance, D.A.B., Currie, B.J., Limmathurotsakul, D., Wiersinga, W.J., 2022. Lancet Infect. Dis. 22 (6), e176–e182.
Secor, P., Dandekar, A., 2020. mBio 11. Doi 10, 00041-00020.
Selan, L., Berlutti, F., Passariello, C., Thaller, M., Renzini, G., 1992. J. Clin. Microbiol. 30 (7), 1739–1742.
Sharma, S., Chatterjee, S., Datta, S., Prasad, R., Dubey, D., et al., 2017. Folia Microbiol. 62, 17–55.
Suttisunhakul, V., Wuthiekanun, V., Brett, P.J., Khusmith, S., Day, N.P., et al., 2016. J. Clin. Microbiol. 54 (5), 1259–1268.
Torres, A.G., Wagner, G.E., Föderl-Höbenreich, E., Assig, K., Lipp, M., et al., 2020. PLoS Neglected Trop. Dis. 14 (7).
Wang, Y., Li, X., Dance, D.A.B., Xia, H., Chen, C., et al., 2022. Infect. Dis. Poverty. 11 (1).
Watthanaworawit, W., Roberts, T., Hopkins, J., Gassiep, I., Norton, R., et al., 2021. BMC Microbiol. 21 (1), 213.
Wiersinga, W.J., Virk, H.S., Torres, A.G., Currie, B.J., Peacock, S.J., et al., 2018. Nat. Rev. Dis. Prim. 4 (1), 1–22.
Xiong, Y., Zhang, J., Yang, Z., Mou, Q., Ma, Y., et al., 2019. J. Am. Chem. Soc. 142 (1), 207–213.
Yao, J., Zhang, Z., Tian, S., Luo, N., Tan, J., et al., 2023. Microbiol. Spectr. 11 (6), e0112523.
Zhang, Z., Wang, C., Zhang, L., Meng, Q., Zhang, Y., et al., 2017. Anal. Methods 9 (36), 5378–5387.